

# Eliminating Spectral Distinguishability in Ultrafast Spontaneous Parametric Down-conversion

Hou Shun Poh<sup>1</sup>, Jiaqing Lim<sup>1</sup>, Ivan Marcikic<sup>2</sup>, Antía Lamas-Linares<sup>1</sup>, and Christian Kurtsiefer<sup>1</sup>

<sup>1</sup>Centre for Quantum Technologies and Department of Physics,

National University of Singapore, 3 Science Drive 2, Singapore 117543

<sup>2</sup>Temasek Laboratories, National University of Singapore, Singapore, 117508

(Dated: December 17, 2018)

Generation of polarization-entangled photon pairs with a precise timing through down-conversion of femtosecond pulses is often faced with a degraded polarization entanglement quality. In a previous experiment we have shown that this degradation is induced by spectral distinguishability between the two decay paths, in accordance with theoretical predictions. Here, we present an experimental study of the spectral compensation scheme proposed and first implemented by Kim *et al.* [1]. By measuring the joint spectral properties of the polarization correlations of the photon pairs, we show that the spectral distinguishability between the down-converted components is eliminated. This scheme results in a visibility of  $97.9 \pm 0.5\%$  in the complementary polarization basis without any spectral filtering.

Spontaneous parametric down-conversion (SPDC) has been widely used to generate entangled photons required in various quantum information protocols [2]. In some experiments, light from continuous-wave lasers is used to pump the SPDC process [3, 4, 5]. These sources can be very bright and provide photon pairs in maximally entangled states with high fidelity in various degrees of freedom [6, 7], making them suitable for applications such as quantum key distribution [8] and fundamental tests of quantum physics (e.g. tests of Leggett models [9, 10]).

For experiments which require photon pairs to exhibit tight localization in time [11, 12], or for preparation of entangled states between more than two photons [13, 14], the SPDC process needs to be pumped by ultrafast optical pulses. Such sources often exhibit a reduction in the quality of polarization entanglement arising from spectral distinguishability of the possible decay paths. This has been addressed theoretically [15, 16, 17]; more recently, experiments investigating the underlying phenomenon have been performed [18, 19, 20, 21, 22]. Various techniques are implemented to eliminate spectral distinguishability: they range from specific tailoring of the down-conversion medium [23], double-pass configuration of the pump beam [24] to interferometric setups [25].

In previous work, we have shown that the wider spectral distribution of ordinarily (*o*) polarized down-converted light in comparison with the extraordinary (*e*) component translates into a spectral distinguishability between the two decay paths for type-II SPDC [21]. When only the polarization degree of freedom is considered, this spectral distinguishability reduces the purity of a state and thus the entanglement quality. Typically, strong spectral filtering is applied in order to detect only photons which fall into the non-distinguishable part of the spectrum. However, any form of spectral filtering drastically reduces the count rate. This is especially disadvantageous in multi-photon experiments where the coincidence rate decreases rapidly with any filter loss. A scheme that can eliminate the spectral distinguishability without significant loss of signal will benefit these experi-

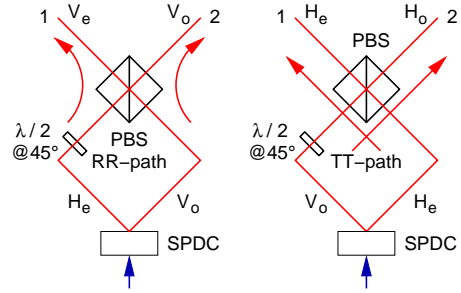


FIG. 1: (Color online) The possible paths of the photon pair generated in spontaneous parametric down conversion (SPDC) for the two corresponding down-converted components. The *e* and *o* polarized photons will exit at the different ports of the PBS independent of their polarization.

ments greatly. One of the ways to overcome this problem is the spectral compensation scheme proposed and first implemented by Kim *et al.* [1]. In this report we will present a detailed experimental study of the effectiveness of this method.

In the “classic” method of generating polarization-entangled photon pairs in non-collinear type-II parametric down conversion, photon pairs are collected at the intersection of the *e* and *o* polarized emission cones [5]. Their combined state covering polarization, direction, and spectral fingerprint can be written as

$$|\Psi\rangle = \frac{1}{\sqrt{2}} (|H_e\rangle_1 |V_o\rangle_2 + e^{i\delta} |V_o\rangle_1 |H_e\rangle_2), \quad (1)$$

where  $\delta$  is the free phase between the states  $|H_e\rangle_1 |V_o\rangle_2$  and  $|V_o\rangle_1 |H_e\rangle_2$  corresponding to the two conversion paths.

In the spectral compensation scheme (Fig. 1), a half-wave plate ( $\lambda/2$ ) placed in one of the arm rotates the polarization by  $90^\circ$ , such that both photons arrive at the polarization beam splitter (PBS) with the same polarization. The  $|H_e\rangle_1 |V_o\rangle_2$  combination is transformed

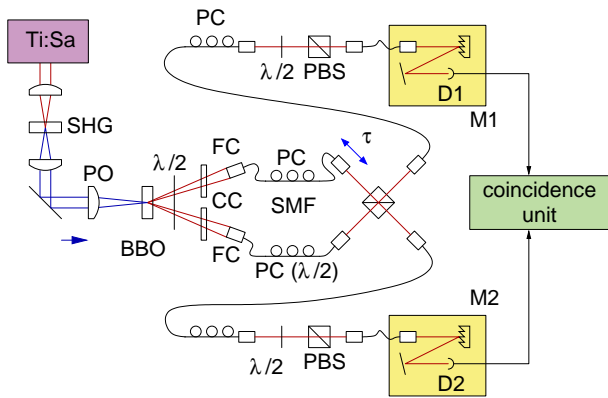


FIG. 2: (Color online) Experimental set-up. Photon pairs generated via SPDC in a nonlinear crystal (BBO) pumped by femtosecond optical pulses are collected into single-mode optical fibers (SMF). A half-wave plate ( $\lambda/2$ ) and polarizing beam splitter (PBS) combination renders them spectrally indistinguishable. The down-converted photons then pass through polarization filters and subsequent grating monochromators for analysis.

into  $|V_e\rangle_1|V_o\rangle_2$ , so both photons are reflected by the PBS (RR path), while the  $|V_o\rangle_1|H_e\rangle_2$  combination is transformed into  $|H_e\rangle_1|H_o\rangle_2$ , so both photons are transmitted by the PBS (TT path). Regardless of their polarization state, photons carrying the spectral fingerprint of  $o$  and  $e$  polarization from the original conversion process will always emerge at a corresponding port of the PBS. As long as there is no path difference between the down conversion crystal and the PBS, neither the arrival time nor the spectrum of the photon will reveal information of the input polarization state, decoupling the temporal and spectral degree of freedom from the polarization. The  $o$  and  $e$  polarized photons need not arrive strictly simultaneously at the PBS for the scheme to work, as shown in various two-photon interference experiments [26, 27]. Similarly to the Hong-Ou-Mandel interference of photon pairs [28], this scheme does not require path length stability to a fraction of the wavelength, but only to a fraction of the coherence length of the photons. It is also simple in the sense that it requires no special engineering of the down-conversion medium or complex double-pass setups. For a free phase  $\delta = \pi$ , the photon pairs are in the Bell state

$$|\Phi^-\rangle = \frac{1}{\sqrt{2}} (|H\rangle_1|H\rangle_2 - |V\rangle_1|V\rangle_2), \quad (2)$$

which we will investigate for the rest of the paper.

We implemented a polarization-entangled photon pair source using type-II phase matching in a crossed-ring configuration [5] and use polarization filters and grating monochromators to resolve the different spectral components for both photons (Fig. 2).

The output of a Ti:Sapphire (Ti:Sa) laser with a repetition rate of 76 MHz is frequency doubled (SHG) to

pulses at  $\bar{\lambda}_p = 390$  nm with a spectral bandwidth of  $\Delta\lambda_p \approx 1.6$  nm full width at half maximum (FWHM). This light beam (average power 900 mW) is corrected for astigmatism and collimated to a waist of  $60 \mu\text{m}$  by the pump optics (PO). At the focus, a 2 mm thick Beta-Barium-Borate (BBO) crystal cut for type-II phase matching with the extraordinary axis aligned to the vertical polarization of the pump is used for down-conversion. A combination of a  $\lambda/2$  and a pair of compensation crystals (CC) eliminates the temporal and transverse walk-off [5]. The free phase  $\delta$  is adjusted by tilting the CC. Down-converted photons are collected into single mode optical fibers (SMF) with a spatial mode diameter matched to that of the pump [29, 30]. Polarization controllers (PC) ensure that the SMF do not affect the polarization of the collected photons.

In one of the spatial modes, the PC is adjusted such that the SMF rotates the polarization by  $90^\circ$ . Both spatial modes are then overlapped in a PBS. The relative propagation delay  $\tau$  to the PBS is adjusted by varying the optical distance for one of the spatial modes. For  $\tau = 0$ , the two decay paths are rendered temporally and spectrally indistinguishable, leaving the photon pair in a pure polarization state  $|\Phi^-\rangle$ . This behavior is shown in Fig. 3, where the coincidences between photons exiting from the PBS are analyzed in an orthogonal basis as a function of the delay, showing a characteristic bump and dip at the point of maximal overlap.

Polarization analysis in each arm is performed by a combination of a  $\lambda/2$  and a PBS, allowing projections onto any arbitrary linear polarization. We denote the direction of these linear polarizations by their rotation  $\alpha_1$  and  $\alpha_2$  with respect to vertical. The transmitted photons are transferred to grating monochromators (M1, M2) with a resolution of 0.3 nm FWHM, and detected with passively quenched Silicon avalanche photodiodes (D1, D2). The detector signals are analyzed for coincidences within a time window shorter than the repetition period of the pump laser.

When sending the photons collected after the compensation scheme into detectors D1 and D2, a coincidence rate of  $105480 \text{ s}^{-1}$  is observed. The total coupling and detection efficiency (calculated from the ratio of pair coincidences to single detector events in one arm) is 10.1%.

To probe the quality of polarization entanglement between the photon pairs, polarization correlations in two bases are measured. Conventionally, the natural basis (i.e., the one aligned to the crystal axes) and a conjugate basis are chosen, for our case the H/V and  $+45^\circ/-45^\circ$  basis, respectively. In the H/V basis, we expect to see nearly perfect correlations due to the type-II conversion process. In the  $+45^\circ/-45^\circ$  basis, the level of (anti-)correlation will depend on the degree of indistinguishability between the two decay paths. For  $|\Phi^-\rangle$ , perfect anti-correlation in the  $+45^\circ/-45^\circ$  basis is expected, but residual distinguishability of the decay paths will deteriorate this.

To assess the degree of distinguishability, coincidences

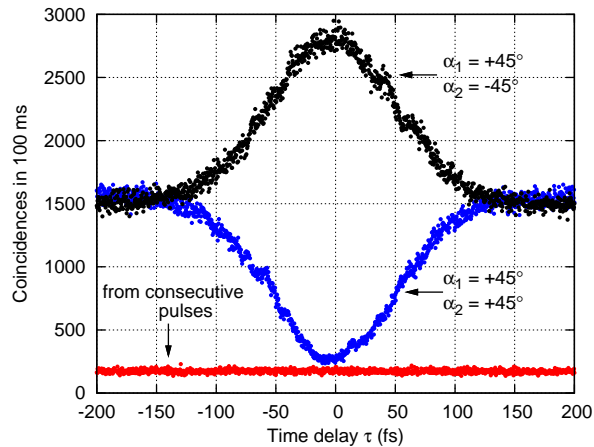


FIG. 3: (Color online) Polarization correlations measured in the  $+45^\circ/-45^\circ$  basis as a function of delay  $\tau$ . Polarization analyzers were oriented at  $\alpha_1 = -\alpha_2 = +45^\circ$  for the bump and at  $\alpha_1 = \alpha_2 = +45^\circ$  for the dip. The bottom trace represents pair coincidences from consecutive pulses. Without correcting for higher order contribution, the visibility of the dip is  $85 \pm 2\%$ . The band of confidence for the corrected value is  $[90 \pm 2\%, 96 \pm 3\%]$ . Refer to the later text for details on the correction procedure.

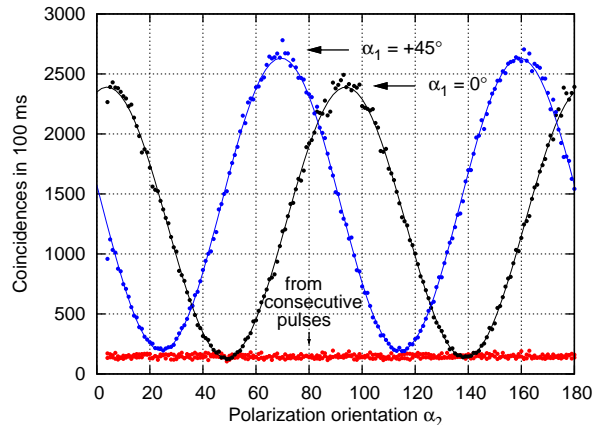


FIG. 4: (Color online) Polarization correlations in the H/V and  $+45^\circ/-45^\circ$  bases. The bottom trace represents pair coincidences from consecutive pulses. Without correcting for any higher order contribution, we observed direct visibilities of  $V_{HV} = 90.0 \pm 0.4\%$  and  $V_{45} = 86.8 \pm 0.4\%$ .

between the detectors over a range of delays  $\tau$  are recorded for  $\alpha_1 = -\alpha_2 = +45^\circ$ . The result is shown in Fig. 3, which reveals clearly a bump for  $\tau = 0$ . A fit to a Gaussian distribution reveals a FWHM of approximately 100 fs, corresponding to the coherence time of the down-converted photons. By choosing  $\alpha_1 = \alpha_2 = +45^\circ$ , a corresponding dip in coincidences is observed. From Fig. 3, the maximal visibility of the dip is  $85 \pm 2\%$ .

The polarization entanglement of the photon pairs was

characterized by measuring the visibilities  $V_{HV}$  and  $V_{45}$  in the H/V and  $+45^\circ/-45^\circ$  basis, respectively. We obtain  $V_{HV}$  ( $V_{45}$ ) by fixing  $\alpha_1$  at  $0^\circ$  ( $+45^\circ$ ), and rotating the orientation of the other analyzer while recording the coincidences. Without spectral filtering, we obtain results  $V_{HV} = 90.0 \pm 0.4\%$  and  $V_{45} = 86.8 \pm 0.4\%$  (see Fig. 4).

However, due to the high instantaneous power involved in the femtosecond-pumped down-conversion, higher order processes (mainly four-photon generation) become significant, and it is important to quantify their contribution. When observing only two-fold coincidences, this four-photon contribution will lead to uncorrelated events lowering the two-photon visibilities. To estimate this four-photon contribution, we record coincidences between consecutive pulses in the same run. Following an argument put forward in [31], the coincidence rate between consecutive pulses is the same as the rate of distinguishable pairs generated in the same pulse. If the two photon pairs are indistinguishable, the four-photon contribution to the two-photon coincidence rate will be half of the pair coincidence rate between consecutive pulses. This allows us to come up with a lower and upper bound for the four-photon generation rate in the setup. Correcting for this higher order contribution, we obtain bands of confidence for the visibilities,  $V_{HV} \in [95.1 \pm 0.5\%, 100.8 \pm 0.5\%]$  and  $V_{45} \in [92.0 \pm 0.4\%, 97.9 \pm 0.5\%]$  for the process leading to pairs only.

Both the bounds for  $V_{45}$  are significantly higher than the results obtained without spectral compensation [21], where we see  $V_{45} \in [69.1 \pm 0.3\%, 72.9 \pm 0.3\%]$  without spectral filtering, and  $V_{45} \in [83.1 \pm 0.3\%, 85.9 \pm 0.3\%]$  with spectral filtering. This shows that the spectral compensation scheme has eliminated the distinguishability between the two down-converted components.

To provide a consistency check for the correction procedure, measurements of the visibilities are made with various pump powers. A model describing the dependence of visibility on pump power is described in [32]. It assumes that the detected pair rate has a contribution  $R_2$  from pairs generated in the same birth process, and a contribution  $R_4$  from partially detected, incoherent double pair events. They can be written as

$$\begin{aligned} R_2 &= P_{\text{pair}} \frac{1 + \cos \theta}{2}, \\ R_4 &= 4 P_{\text{double pair}} \frac{2 + \cos \theta}{4}, \end{aligned} \quad (3)$$

where  $\theta = \alpha_1 - \alpha_2$ , and  $P_{\text{pair}}$  and  $P_{\text{double pair}}$  are the probabilities for creating a pair and an incoherent double pair per pulse, respectively. The first one can be written as

$$P_{\text{pair}} = \frac{S}{\eta_c \eta_q f}, \quad (4)$$

where  $S$  is the rate of detector events on one side,  $\eta_c$  characterizes the coupling efficiency,  $\eta_q$  is the quantum efficiency of the detectors, and  $f$  the repetition rate of the

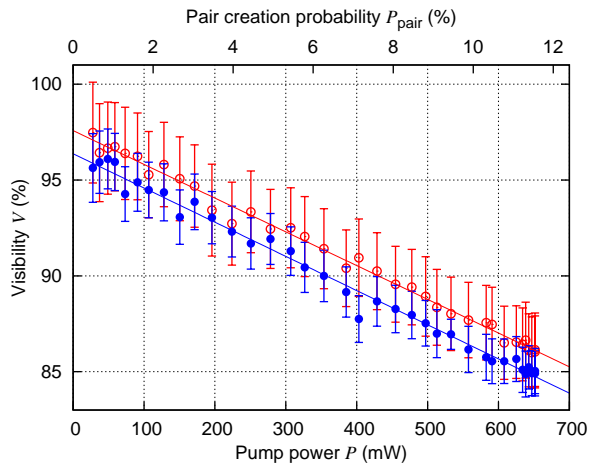


FIG. 5: (Color online) Visibility  $V_{HV}$  (open circles) and  $V_{45}$  (solid circles) measured as a function of the pump power. The probability of creating a pair  $P_{\text{pair}}$  (top axis) is proportional to the pump power. Solid lines show linear fits to the visibility reduction. From the slope, a pair generation probability can be derived via Eq. 5 (top axis). At low power, the coincidences are dominated by the contribution from first order down-conversion. The extrapolated visibilities at  $P = 0$   $V_{HV} = 97.6 \pm 0.1\%$  and  $V_{45} = 96.4 \pm 0.1\%$ .

laser. Assuming a Poissonian distribution in the counting of incoherent pairs events, one finds  $P_{\text{double pair}} = P_{\text{pair}}^2/2$ . The visibility  $V$  obtained from the sum of  $R_2$  and  $R_4$  is

$$V \approx V_{\text{max}} - P_{\text{pair}}, \quad (5)$$

with  $V_{\text{max}}$  being the limit for the visibility at low pump power. Figure 5 shows the visibilities observed for different pump powers, exhibiting a linear decrease with power as expected according to Eq. 5. The slope of both visibility measurements coincide ( $0.0177 \pm 0.0003\% \text{ mW}^{-1}$ ) and allows to rescale power into pair probability (see top axis on figure). From the pair probability and a single detector event rate (corrected for saturation effects), a combined detector/coupling efficiency of 11.3% can be derived via Eq. (4).

The limit  $V_{\text{max}}$  for the visibility at low pump power are  $V_{HV} = 97.6 \pm 0.1\%$  and  $V_{45} = 96.4 \pm 0.1\%$  in agreement with results from the correction procedure.

To understand the joint spectral properties of the polarization correlations, we measured the joint spectrum of the photon pairs generated from each of the two decay paths. This is done by fixing the polarization analyzers to the natural basis of the down-conversion crystal, selecting either the  $H_1H_2$  or  $V_1V_2$  decay path. The spectra are taken with a resolution of 0.5 nm and an integration time of 30 s for each wavelength pair.

Our results (shown in Fig. 6) have nearly identical distributions, with the exception of their maximum coincidence rate. A balanced contribution between the  $H_1H_2$  and  $V_1V_2$  decay path is found at all wavelength pairs,

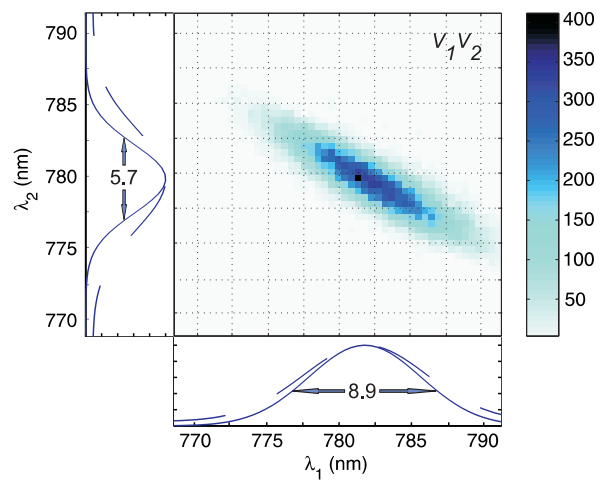
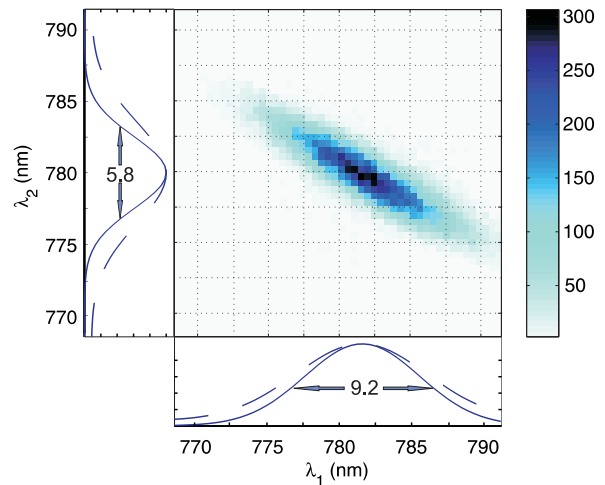


FIG. 6: (Color online) Joint spectra of coincidence counts in 30 s for  $H_1H_2$  (upper panel) and  $V_1V_2$  (lower panel) polarizations. The spectra corresponding to the two decay paths  $RR$  and  $TT$  are almost identical with the exception of the difference in the maximum count rate recorded. Differences between the widths of the marginal (solid trace) and the single photon spectra (dashed traces), as well as between the  $e$  and  $o$  polarization are observed as expected.

compatible with state  $|\Phi^-\rangle$  at every point. This is in contrast with results obtained without spectral compensation [21], with the different spectral fingerprints of the two decay paths.

The marginal distributions  $\lambda_1$ ,  $\lambda_2$  exhibit widths of  $\Delta\lambda_{m1} = 9.2 \pm 0.3 \text{ nm}$ ,  $\Delta\lambda_{m2} = 5.8 \pm 0.2 \text{ nm}$  (FWHM) for the  $H_1H_2$  combination. A comparable distribution is also observed for the  $V_1V_2$  joint spectrum (Fig. 6, lower panel). Thus, the spectral degree of freedom no longer reveals any information on the corresponding polarization state.

The spectral distribution of the photons collected in each spatial mode obtained from the same run have central wavelengths of  $\bar{\lambda}_H = 781.55 \pm 0.03 \text{ nm}$  and  $\bar{\lambda}_V =$



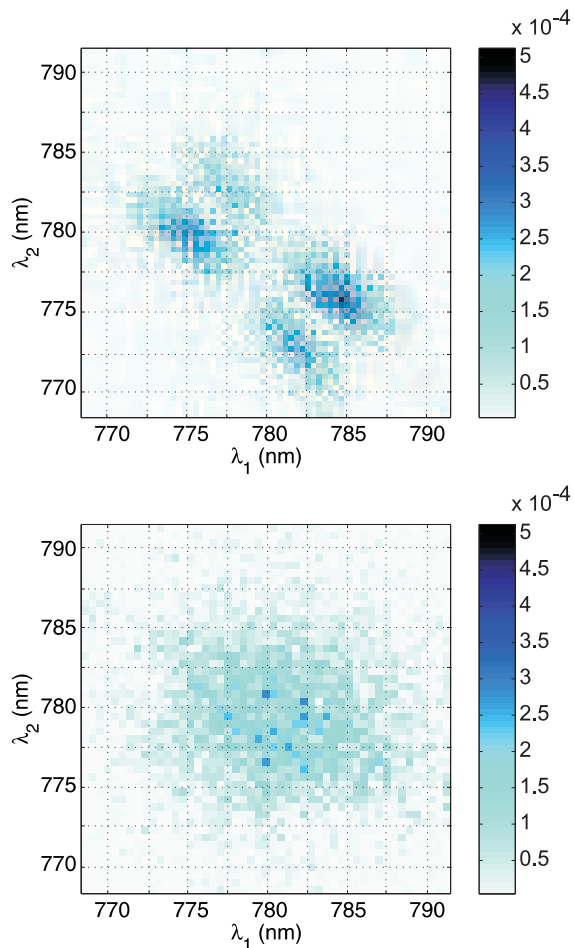


FIG. 7: (Color online) Joint spectra of coincidences measured for the  $+45^\circ/+45^\circ$  polarization combination. The counts are normalized to the total events in the spectral mapping experiments for both configurations. Without the spectral compensation scheme (upper panel), the joint spectrum exhibits four regions of higher count rate, comprising a fraction of 0.14 of all events. They correspond to areas with an imbalance of the two decay paths. With the spectral compensation scheme (lower panel), the joint spectrum, a fraction of 0.10 of the total events, exhibits a distribution of uncorrelated pair events about the degenerate wavelength which is compatible with estimates of the four-photon contribution.

$780.19 \pm 0.01$  nm, and a FWHM of  $\Delta\lambda_H = 10.7 \pm 0.1$  nm and  $\Delta\lambda_V = 8.30 \pm 0.05$  nm, respectively. We note that the single photon spectral distributions (dashed lines in Fig. 6) are wider than the marginals,  $\Delta\lambda_H = 8.3$  nm,  $\Delta\lambda_V = 10.4$  nm. This disparity is caused by the difference in the width of the spectral distribution between the  $e$  and  $o$  polarized photon. In the SPDC process, the spectral distribution of down-converted photons is connected to their angular dispersion. For a certain accep-

tance angle subtended by the collection, the  $e$  polarised photons (which have a narrower spread in the emission direction) will be collected more efficiently than the  $o$  polarized photon. Thus, not every photon detected in one spatial mode has its twin in the other mode [21].

The joint spectra for polarizations in the complementary basis,  $(+45^\circ/+45^\circ)$ , are shown in Fig. 7, normalized to the total events both in the  $+45^\circ/+45^\circ$  and  $+45^\circ/-45^\circ$  basis. The upper panel shows the result without spectral compensation [21] for comparison. It reveals regions with higher rates, indicating an imbalance between the two down-converted components in those areas. With the spectral compensation (lower panel), the distribution of uncorrelated pair events is compatible with the four-photon contribution. This can be seen from the marginal distribution of the joint spectrum,  $\Delta\lambda_{m1} = 10.8 \pm 0.4$  nm,  $\Delta\lambda_{m2} = 8.4 \pm 0.2$  nm (FWHM) which is identical to the distribution of the photon collected in each spatial mode.

To characterize the distinguishability between the two decay paths, we also need to look at the corresponding  $+45^\circ/-45^\circ$  joint spectrum. Together with this measurement, the visibility  $V_{45}$  can be reconstructed by summing over all wavelengths:

$$V_{45} = \frac{\sum_{\lambda_1, \lambda_2} c^{+,-}(\lambda_1, \lambda_2) - \sum_{\lambda_1, \lambda_2} c^{+,+}(\lambda_1, \lambda_2)}{\sum_{\lambda_1, \lambda_2} c^{+,-}(\lambda_1, \lambda_2) + \sum_{\lambda_1, \lambda_2} c^{+,+}(\lambda_1, \lambda_2)}, \quad (6)$$

where the  $c^{+,\pm}(\lambda_1, \lambda_2)$  are coincidence events detected for various wavelength pairs, and  $+-$  and  $++$  refers to the  $+45^\circ/-45^\circ$  and  $+45^\circ/+45^\circ$  polarizer settings.

After correcting for the four-photon contribution, we get  $V_{45} \in [73.8 \pm 0.5\%, 80.2 \pm 0.6\%]$  without spectral compensation. With spectral compensation, we get  $V_{45} \in [89.4 \pm 0.5\%, 100.4 \pm 0.6\%]$ .

In summary, the compensation scheme eliminated the spectral distinguishability between the two decay paths. This is demonstrated by the identical joint spectra measured in the natural basis of the down-conversion and direct correlation measurements at different power levels. The balanced contribution between the two down-conversion paths for all spectral components does not reveal any information about the polarization state, thus entanglement quality is preserved when the spectral degree of freedom is ignored. After taking the higher order contributions into consideration, we achieved a high visibility of  $V_{45} = 97.9 \pm 0.5\%$  in the complementary basis without the need of spectral filtering. The simplicity and effectiveness of this scheme make it a useful addition to the toolkit of techniques used for efficiently preparing entangled states of two and more photons.

This work is supported by the National Research Foundation & Ministry of Education, Singapore, and ASTAR under SERC grant No. 052 101 0043.

[1] Y.-H. Kim and W. P. Grice, *J. Mod. Opt.* **49**, 2309 (2002)

[2] D. Bouwmeester, A. Ekert, and A. Zeilinger, *The physics*

- of quantum information* (Springer, 2001).
- [3] D. C. Burnham and D. L. Weinberg, *Phys. Rev. Lett.* **25**, 84 (1970).
- [4] D. N. Klyshko, *Photons and Nonlinear Optics* (Gordon and Breach Science Publishers, New York, 1989).
- [5] P. G. Kwiat, K. Mattle, H. Weinfurter, A. Zeilinger, A. V. Sergienko, and Y. Shih, *Phys. Rev. Lett.* **75**, 4337 (1995).
- [6] J. Brendel, E. Mohler, and W. Martienssen, *Europhys. Lett.* **20**, 575 (1992).
- [7] P. G. Kwiat, E. Waks, A. G. White, I. Appelbaum, and P. H. Eberhard, *Phys. Rev. A* **60**, R773 (1999).
- [8] T. Jennewein, C. Simon, G. Weihs, H. Weinfurter, and A. Zeilinger, *Phys. Rev. Lett.* **84**, 4729 (2000).
- [9] S. Gröblacher, T. Paterek, R. Kaltenbaek, C. Brukner, M. Żukowski, M. Aspelmeyer, and A. Zeilinger, *Nature* **446**, 871 (2007).
- [10] C. Branciard, N. Brunner, N. Gisin, C. Kurtsiefer, A. Lamas-Linares, A. Ling, and V. Scarani, *Nature Phys.* **4**, 681 (2008).
- [11] D. Bouwmeester, J.-W. Pan, K. Mattle, M. Eibl, H. Weinfurter, and A. Zeilinger, *Nature (London)* **390**, 575 (1997).
- [12] A. Lamas-Linares, J.C. Howell, C. Simon, and D. Bouwmeester, *Science* **296**, 712 (2002).
- [13] S. Gaertner, M. Bourennane, M. Eibl, C. Kurtsiefer, and H. Weinfurter, *Appl. Phys. B* **77**, 803 (2003).
- [14] A. M. Goebel, C. Wagenknecht, Q. Zhang, Y.-A. Chen, K. Chen, J. Schmiedmayer, and J.-W. Pan, *Phys. Rev. Lett.* **101**, 080403 (2008).
- [15] T. E. Keller and M. H. Rubin, *Phys. Rev. A* **56**, 1534 (1997).
- [16] W. P. Grice and I. A. Walmsley, *Phys. Rev. A* **56**, 1627 (1997).
- [17] W. P. Grice, R. Erdmann, I. A. Walmsley, and D. Branning, *Phys. Rev. A* **57**, R2289 (1998).
- [18] M. Atatüre, A. V. Sergienko, B. M. Jost, B. E. S. Saleh, and M. C. Teich, *Phys. Rev. Lett.* **83**, 1323 (1999).
- [19] Y.-H. Kim and W. P. Grice, *Opt. Lett.* **30**, 908 (2005).
- [20] W. Wasilewski, P. Wasylczyk, P. Kolenderski, K. Banaszek, and C. Radzewicz, *Opt. Lett.* **31**, 1130 (2006).
- [21] H. S. Poh, C. Y. Lum, I. Marcikic, A. Lamas-Linares, and C. Kurtsiefer, *Phys. Rev. A* **75**, 043816 (2007).
- [22] M. Avenhaus, M. V. Chekhova, L. A. Leuchs, and C. Silberhorn, *Phys. Rev. A* **79**, 043836 (2009).
- [23] R. Erdmann, D. Branning, W. P. Grice, and I. A. Walmsley, *Phys. Rev. A* **62**, 053810 (2000).
- [24] J. F. Hodelin, G. Khoury, and D. Bouwmeester, *Phys. Rev. A* **74**, 013802 (2006).
- [25] D. Branning, W. P. Grice, R. Erdmann, and I. A. Walmsley, *Phys. Rev. Lett.* **83**, 955 (1999).
- [26] T. B. Pittman, D. V. Strekalov, A. Migdall, M. H. Rubin, A. V. Sergienko, and Y. Shih, *Phys. Rev. Lett.* **77**, 1917 (1996).
- [27] Y.-H. Kim, *Phys. Lett. A* **315**, 352 (2003).
- [28] C. K. Hong, Z. Y. Ou, and L. Mandel, *Phys. Rev. Lett.* **59**, 2044 (1987).
- [29] C. Kurtsiefer, M. Oberparleiter, and H. Weinfurter, *Phys. Rev. A* **64**, 023802 (2001).
- [30] F. A. Bovino, P. Varisco, A. M. Colla, G. Castagnoli, G. D. Giuseppe, and A. V. Sergienko, *Opt. Commun.* **227**, 343 (2003).
- [31] H. de Riedmatten, V. Scarani, I. Marcikic, A. Acin, W. Tittel, H. Zbinden, and N. Gisin, *J. Mod. Opt.* **51**, 1637 (2004).
- [32] I. Marcikic, H. de Riedmatten, W. Tittel, V. Scarani, H. Zbinden, and N. Gisin, *Phys. Rev. A* **66**, 062308 (2002).